Original Article

SPIO-loaded nanostructured lipid carriers as liver-targeted molecular T2-weighted MRI contrast agent

Xiuliang Zhu[1#], Xueying Deng[2#], Chenying Lu[1#], Ying Chen[1], Liyong Jie[1], Qian Zhang[1], Wei Li[3], Zuhua Wang[4], Yongzhong Du[3], Risheng Yu[1]

[1]Department of Radiology, The Second Affiliated Hospital, Zhejiang University School of Medicine, Hangzhou 310009, China; [2]Department of Radiology, Zhejiang Cancer Hospital, Hangzhou 310022, China; [3]Institute of Pharmaceutics, College of Pharmaceutical Sciences, Zhejiang University, Hangzhou 310058, China; [4]College of Pharmaceutical Sciences, Guiyang College of Traditional Chinese Medicine, Guiyang 550002, China

[#]These authors contributed equally to this work.

Correspondence to: Risheng Yu. Department of Radiology, The Second Affiliated Hospital, Zhejiang University School of Medicine, 88# Jiefang Road, Hangzhou 310009, China. Email: risheng-yu@zju.edu.cn; Yongzhong Du. Institute of Pharmaceutics, College of Pharmaceutical Sciences, Zhejiang University, 866 Yu-Hang-Tang Road, Hangzhou 310058, China. Email: duyongzhong@zju.edu.cn; Zuhua Wang. College of Pharmaceutical Sciences, Guiyang College of Traditional Chinese Medicine, Guiyang 550002, China. Email: wangrui551601@163.com.

Background: Superparamagnetic iron oxide (SPIO) acts as a negative contrast agent in magnetic resonance imaging (MRI), and is widely used in clinical applications, including the diagnosis of hepatic diseases. Hepatocyte-targeted magnetic resonance contrast agents (MRCAs) can provide useful information for evaluating hepatic diseases. We prepared targeted magnetic nanostructured lipid carriers (MNLCs) to enhance the hepatocytes targeting efficiency.
Methods: *In vitro* characterizations of MNLCs were determined by transmission electron microscopy (TEM). The cytotoxicity assay of the MNLCs was measured by methyl tetrazolium (MTT) method. The uptaken study was measured by confocal microscopy, flow cytometry and MRI *in vitro*. The enhanced liver-targeting efficiency of MNLCs was measured by fluorescence imaging and MRI *in vivo*.
Results: Gal-NLC-SPIO was prepared successfully. The cytotoxicity assay of the MNLCs demonstrated that the MNLC had relatively low cytotoxicity and high biocompatibility for LO2 cells. More importantly, we confirmed that Gal-NLC-SPIO had greater uptake by LO2 cells than Gal-NLC-SPIO/PEG and free Gal *in vitro*. A liver distribution study of MNLCs in normal mice demonstrated that the fluorescent signal values to livers of the Gal-NLC-SPIO were significantly stronger than those of NLC-SPIO and Gal-NLC-SPIO/PEG. The liver targeting efficiency of Gal-NLC-SPIO was confirmed both *in vitro* and *in vivo*.
Conclusions: We successfully developed liver-targeting MNLCs, which showed accurate hepatocytes targeting, and thus have the potential to be a new MRI contrast agent to help the diagnosis of liver diseases.

Keywords: Superparamagnetic iron oxide (SPIO); magnetic resonance imaging (MRI); solid lipid nanoparticle galactose (SLN galactose); liver-targeted

Introduction

Magnetic resonance imaging (MRI), because of its high spatial, high temporal resolution, non-ionizing radiation and multiparameter imaging, is widely used in clinical diagnosis and research as a non-invasive and effective imaging technique, especially for early cancer diagnosis (1,2). In order to provide more detailed abnormality images and to distinguish diagnostic interest regions from background

tissues, magnetic resonance contrast agents (MRCAs) are widely utilized (3-5). MRCAs are used to alter the water molecules' relaxation times and subsequently to the increase tissue contrast on relaxation-weighted imaging sequences (6). Furthermore, hepatocyte-targeted MRCAs can used to evaluate hepatic diseases, such as hepatic tumor and hepatitis, because hepatic diseases can reduce the hepatocyte-targeted imaging agent uptaken into hepatocytes. Therefore, hepatic diseases can be better evaluated *in vivo* by using hepatocyte-targeted MRCAs (7), of which there are two types. One type, T1 MRCA typically incudes gadolinium (Gd) complexes and manganese (Mn) oxide nanoparticles, also called positive MRCAs, which present hyperintensity in T1-weighted images (8,9). The classic examples of T2 MRCAs include superparamagnetic iron oxide nanoparticles (SPIO), also called negative MRCAs, which present hypointensity in T2-weighted images (10,11). The potential use of SPIO as MRI probes has been widely studied with regard to their suitable magnetic properties, good biocompatibility and non-toxicity. Their outlook is promising because SPIO can display magnetic behavior in the presence of the magnetic field, and so can be productively applied *in vivo* and *in vitro* (10-12).

Drug targeted delivery systems are widely found in nanomedicine, and can be used to prolong, localize, and target specific designated tissue parts of the body (13-18), and they are consist of active targeted drug delivery (e.g., targeted to hepatic tumor or normal liver) and passive targeted drug delivery (e.g., engulfed by reticuloendothelial system, RES) (15-18). Contrast agent targeted delivery systems, like drug targeted delivery systems, are becoming more popular used for targeting diagnosis of disease (18).

Lipid based nanoparticles, with poorly water-soluble and low toxicity, have been used as amphiphilic nanocarriers in recent years (19-23). The nanostructured lipid carrier (NLC) is a novel nanoparticle delivery system, composed of a solid lipid and an oil phase, which enables a higher drug loading capacity and stability when compared to solid lipid nanoparticles (SLNs) (21-23). This is possible because the NLC's strong hydrophobic surface, after intravenous injection into the body, soon to be swallowed by RES, and into the liver and spleen by passive targeting (24,25).

In addition, for the purpose of specifically targeting tumor tissue, NLCs can be modified with antibodies or ligand (26-28). Mammalian hepatocytes have large numbers of high-affinity and cell-surface receptors (asialoglycoprotein receptor, ASGPR) which can bind to asialoglycoproteins and can specifically recognize ligands with terminal galactose residues. Each liver cell has more than 5×10^5 receptors in a normal liver, but the number and function of the receptors declines from hepatitis, cirrhosis, liver cancer and other liver diseases. Galactose (Gal) is a hepatocyte-specific ligand of ASGPR and the liver targeting group, which has potential to induce and improve cell adhesion and the performance of liver extracellular matrix scaffold (27,28).

In this study, galactose-conjugated nanostructured lipid carriers (Gal-NLCs) were prepared as a hepatocyte-targeting imaging probe to deliver magnetic SPIO nanoparticles (i.e., SPIO loaded Gal-NLC, Gal-NLC-SPIO), which could passively and actively target the liver due to active targeting modification with galactose in the nano-carrier (*Figure 1*). Then, the targeting ability of nanoparticles to normal liver cells and hepatoma cells was further investigated, while the diagnostic efficiency of hepatocellular carcinoma *in vivo* and *in vitro* was also evaluated.

Methods

Cell culture

RAW264.7 cells (mouse macrophage cell line), LO2 cells (human hepatic cell line) and HepG2 cells (human hepatocellular carcinoma cell line) were investigated in this study. The cells were maintained in DMEM at 37 ℃ in a humidified atmosphere of 5% CO_2. All the mediums contained fetal bovine serum (FBS) [10% (v/v)], and 1% streptomycin/penicillin.

Synthesis of Gal-ODA

The Gal-ODA conjugate was synthesized by the acylation between the carboxyl group of lactobionic acid (LA) derived from the lactose and amino group of ODA. LA was coupled with ODA using 1-ethyl-3-(3-dimethyl aminopropyl) carbo-diimide hydrochloride (EDC) as the coupling agent. Briefly, 1 g of LA, 0.5 g of ODA and 1.76 g of EDC were dissolved in 50 mL of ethanol solution in a water bath at 60 ℃ for 24 h. The final products were further purified and followed by lyophilization, and the Gal-ODA was finally extracted.

Preparation of magnetic nanostructured lipid carriers (MNLC)

Galactose-conjugated MNLC (NLC-SPIO, Gal-NLC-SPIO and Gal-NLC-SPIO/PEG) was prepared using the
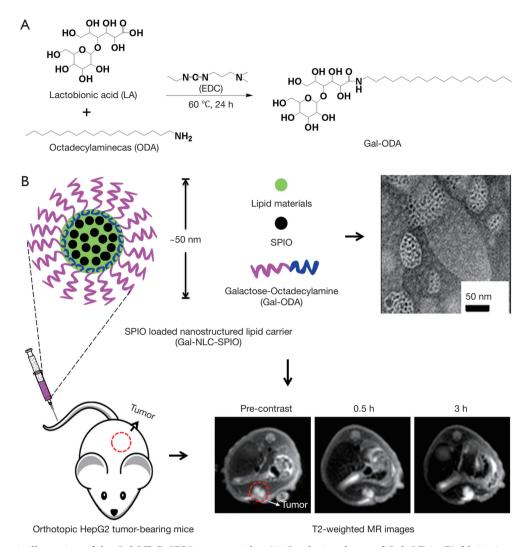
Figure 1 Schematic illustration of the Gal-NLC-SPIO nanoparticles. (A) Synthetic scheme of Gal-ODA; (B) fabrication procedure of Gal-NLC-SPIO nanoparticles and further liver molecular MRI imaging. Gal-NLC, galactose-conjugated nanostructured lipid carrier; SPIO, superparamagnetic iron oxide.

solvent diffusion method. Briefly, Fe_3O_4 dispersion (1 mL) was added into 0.1% Poloxamer 188 (47 mL) in deionized water solution using a probe sonicator (600 W, Sonicator JY92-II DN, China) working 2 s following stopping 3 s to form a dispersion of magnetic nanoparticles. Oleic acid in ethanol solution (1 mL, 5 mg/mL) was added and followed by sonication for 5 minutes to stabilize the nanoparticles. Subsequently, 32 mg of monostearin, 32 mg of monostearin +3 mg of Gal-ODA, and 32 mg of monostearin +3 mg of Gal-ODA +3 mg of polyethylene glycol monostearate, were respectively dissolved in ethanol solution (2 mL, 70 ℃), and immediately added into the Fe_3O_4 nanoparticles in an ultrasound water bath (70 ℃) for 10 min to obtain the

magnetic nanoparticles of NLC-SPIO, Gal-NLC-SPIO and Gal-NLC-SPIO/PEG.

Physicochemical characteristics of MNLC

[1]H nuclear magnetic resonance (NMR) spectra were used to analyse the synthesized Gal-ODA. LA, ODA and Gal-ODA were dissolved in D_2O, and measured by NMR spectra. The average diameter and zeta potential of the MNLC were measured with a zetasizer (3000HS, Malvern Instruments Ltd, UK). Morphological examination of the MNLC was performed via transmission electron microscopy (TEM) (JEOL JEM-1230, Japan). Each sample was dropped onto a

copper grid and stained with phosphotungstic acid (2%, w/v) for viewing.

Cytotoxicity assay in vitro

In order to study the cytotoxicity of MNLC, the methyl tetrazolium (MTT) assay was used on the test cells. Three kinds of cells were each briefly seeded onto their own 96-well culture plate at a density of 10,000 cells per well in 200 µL of complete medium. After cultured at 37 ℃ for 24 h, the cells were exposed to a series of concentrations of magnetic nanoparticles for another 48 h. At the end of incubation, cells were incubated with 20 µL MTT solution (5 mg/mL) in each well for a further 4 h at 37 ℃. Finally, the cells were dissolved by dimethyl sulfoxide (DMSO, 100 µL) and the absorbance values were measured at 570 nm using a microplate reader (Bio-Rad, Model 680, USA). All the experiments were performed 3 times. Cell viability was calculated using an MTT assay.

Cellular uptake test of MNLC

The fluorescein isothiocyanate-octadecylamine (FITC-ODA) was prepared according to our previous study (29). As described above, the FITC-labeled MNLC were prepared using FITC-ODA (5 mg) instead of monostearin.

LO2, HepG2 and RAW264.7 cells were seeded onto coverslips in a 24-well plate for 24 h, respectively. Cells were then incubated with FITC labeled MNLC in growth medium for 30 min. The cells were then washed 3 times, and the coverslips were observed under a confocal microscope (LSM-510META, ZEISS, Germany). The quantitative analysis of cellular uptake was further evaluated via a flow-cytometer (FC500MCL, Beckman Coulter, USA).

In vitro MR imaging of MNLC

A 3.0 T clinical MR scanner (GE, Discovery 750, USA) was used for an *in vitro* MR imaging experiment. LO2 and HepG2 cells were incubated with MNLC for 3 h, and then collected in 1.5 mL microcentrifuge tubes by centrifugation. The cells were mixed with agarose gel (0.5%, 200 mL), and T2-weight MR images were obtained using an MR scanner.

In vivo MR imaging studies

Male BALB/C+nu/F1 nude mice were provided by the Zhejiang Medical Animal Centre. All the animal studies were conducted in accordance with the National Institutes of Health (NIH, USA) guidelines for the care and use of laboratory animals and with the approval of the Scientific Investigation Board of Zhejiang University.

Nude mice were implanted with HepG2 cells to establish orthotopic liver cancer models. The abdominal cavity was cut to reveal normal liver tissues, and the wound was then sutured using biodegradable stitches after injecting HepG2 cells (~5×10^6 cells in 20 µL of serum-free DMEM) into the liver parenchyma. About 2 weeks later, mice bearing HepG2 tumors of approximately 2 mm^3 were randomized into 3 groups (n=5 per group), and taken for MR imaging. T2-weighted MR images were obtained before MNLC (200 µL, 100 µg/mL) was injected through each mouse's tail vein. The mice were then imaged again at predetermined times (0, 1, 3 h) after the injection.

Histological analysis

The mice were sacrificed after MR examination, and the livers were collected for histological analysis. The fresh tissues were fixed with 10% paraformaldehyde, and embedded in paraffin. The sections were stained using haematoxylin-eosin (H&E), and examined under a light microscope for histological analysis. The accumulation of iron in the tissues was observed by Prussian blue staining. The microscopic images were observed by a Leica fluorescence microscope.

Statistical analysis

The data were expressed as the mean (standard error) of three separate experiments. Differences between the groups were assessed with Student's *t*-test, and P values less than 0.05 were considered statistically significant.

Results

Structure confirmation of Gal-ODA

The reaction scheme of Gal-ODA is shown in *Figure 1*. The chemical structure of LA, ODA and Gal-ODA were determined by ^{1}H NMR spectra (*Figure S1*). The ^{1}H NMR chemical shift of the proton of carboxyl group for LA (about 12.5) was displaced to about 7.5, equal to the chemical shift of the proton of amide group for Gal-ODA. These results indicate that Gal-ODA was synthesized successfully.
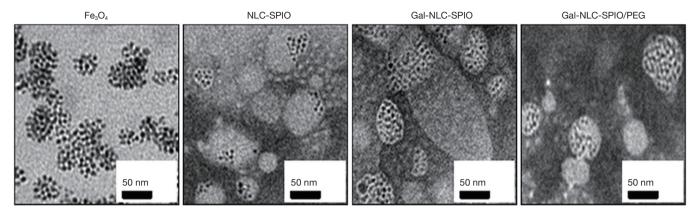
774

Zhu et al. A new MRI contrast agent

Fe$_3$O$_4$ NLC-SPIO   Gal-NLC-SPIO   Gal-NLC-SPIO/PEG

Figure 2 Preparation and characteristics. TEM images of Fe$_3$O$_4$, NLC-SPIO, Gal-NLC-SPIO and Gal-NLC-SPIO/PEG nanoparticles (×100,000, bar =50 nm). TEM, transmission electron microscopy; Gal-NLC, galactose-conjugated nanostructured lipid carrier; SPIO, superparamagnetic iron oxide.

Preparation and physicochemical characteristics of MNLC

The solvent diffusion method was utilized to prepare Gal-NLC-SPIO, NLC-SPIO and Gal-NLC-SPIO/PEG. The morphology and size of MNLC were characterized by zetasizer and TEM. Particle diameter and zeta potential of Gal-NLC-SPIO, NLC-SPIO and Gal-NLC-SPIO/PEG are shown in *Table S1*. The results indicate that 3 magnetic lipid nanoparticles are uniformly distributed (PI <0.3) and have negative charges, with the particle sizes being similar. TEM photographs of Fe$_3$O$_4$, Gal-NLC-SPIO, NLC-SPIO and Gal-NLC-SPIO/PEG are shown in *Figure 2*. The photographs demonstrate the successful entrapment of SPIO into Gal-NLC-SPIO, NLC-SPIO and Gal-NLC-SPIO/PEG, with particle size of approximately 50 nm. The results were similar to that from the zetasizer.

In vitro cytotoxicity

The cytotoxicities of Gal-NLC-SPIO, NLC-SPIO and Gal-NLC-SPIO/PEG were tested by both MTT and cell viability assays. Using LO2, HepG2, and RAW264.7 cell lines as model cells, the results in *Figure S2* illustrate that cell viability was still higher than 80% even when the concentration of Fe$_3$O$_4$ rose to 100 μg·mL^{-1} (nanoparticles was 1 mg·mL^{-1}). This is evidence to the fact that the MNLC had a relatively high biocompatibility and low cytotoxicity for both normal cells and tumor cells.

Uptake of MNLC by cells

In order to study the targeting efficiency of Gal-NLC-SPIO toward LO2 cells, cellular competitive uptake of rhodamine isothiocyanate (RITC), labeled MNLC on LO2/HepG2 cells co-cultured systems, and the targeting efficiency was detected via confocal microscopy (*Figure 3*).

Line 3 in *Figure 3B* shows an obvious difference in the cellular uptake of Gal-NLC-SPIO on the LO2/HepG2 cells co-cultured systems, characterized by more efficient cellular uptake of Gal-NLC-SPIO on LO2 cells compared with HepG2 cells. However, NLC-SPIO and Gal-NLC-SPIO/PEG showed minor uptake on the LO2/HepG2 cells co-cultured systems (line 1 and 2 in *Figure 3B*).

The results of cellular competitive uptake confirmed the specific binding of the Gal-NLC-SPIO to LO2 cells, on account of the presence of an abundant ASGPR on the LO2 cell surface (26-28). The results of qualitative and quantitative cellular uptake for FITC labeled Gal-NLC-SPIO, NLC-SPIO and Gal-NLC-SPIO/PEG were presented (*Figure 4*) after the MNLC were incubated with LO2, HepG2 and RAW264.7 cells for 1 h and 12 h, respectively. The results demonstrated that the SPIO could be internalized into cells mediated by the MNLC. The uptake of the Gal-NLC-SPIO, NLC-SPIO and Gal-NLC-SPIO/PEG by LO2, HepG2 and RAW264.7 cells were time dependent. The SPIO accumulation in RAW264.7 cells by NLC-SPIO was faster than in Gal-NLC-SPIO and Gal-NLC-SPIO/PEG. The SPIO accumulation in LO2 cells by Gal-NLC-SPIO was faster than in NLC-SPIO and Gal-NLC-SPIO/PEG, while there was no significant difference among the magnetic NLCs in HepG2 cells. The cellular uptake data confirmed the specific and strong targeting abilities of the NLC-SPIO to RAW264.7 cells and the Gal-NLC-SPIO to LO2 cells.
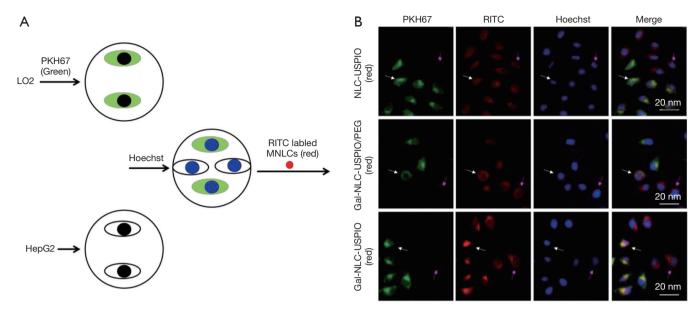
Figure 3 Cellular competitive uptake studies. (A) Schematic diagram of cellular competitive uptake of Gal-NLC-SPIO, NLC-SPIO and Gal-NLC-SPIO/PEG; (B) confocal microscopy images of RITC labeled MNLC for 1 h. LO2 cells (the cytoplasmic membrane labeled with PKH67 fluorescent linker, green) co-cultured with HepG2 cells were incubated with RITC-Gal-NLC-SPIO, RITC-NLC-SPIO and RITC-Gal-NLC-SPIO/PEG (red). The nucleus were all stained with Hoechst 33342. The white arrow stands for LO2 cells, the pink arrow stands for HepG2 cells. (PKH67/FITC, excitation wavelengths 488 nm, emission wavelengths 500–540 nm; RITC, excitation wavelengths 561 nm, emission wavelengths 580–620 nm). Gal-NLC, galactose-conjugated nanostructured lipid carrier; SPIO, superparamagnetic iron oxide; RITC, rhodamine isothiocyanate; MNLC, magnetic nanostructured lipid carrier.

Liver distribution of MNLC in vivo

Liver distribution is an important prerequisite for the diagnosis of liver disease. To further research whether MNLC could target the liver *in vivo*, DiR was loaded in MNLC and used as a fluorescent probe for *in vivo* imaging. After injection of DiR loaded MNLC, accumulation of DiR fluorescence in the liver was time dependent and the fluorescent signal intensity increased gradually. The fluorescence intensity of liver injected by Gal-NLC-SPIO/DiR was stronger than in NLC-SPIO/DiR and Gal-NLC-SPIO/PEG/DiR, as shown in *Figure 5A*. The results in *Figure 5B* also demonstrate that the fluorescent signal values of the Gal-NLC-SPIO to livers were significantly stronger than those of NLC-SPIO and Gal-NLC-SPIO/PEG in livers at every time point, suggesting that Gal-NLC-SPIO has specific targeting ability to liver tissue and has great potential as an MRI contrast agent.
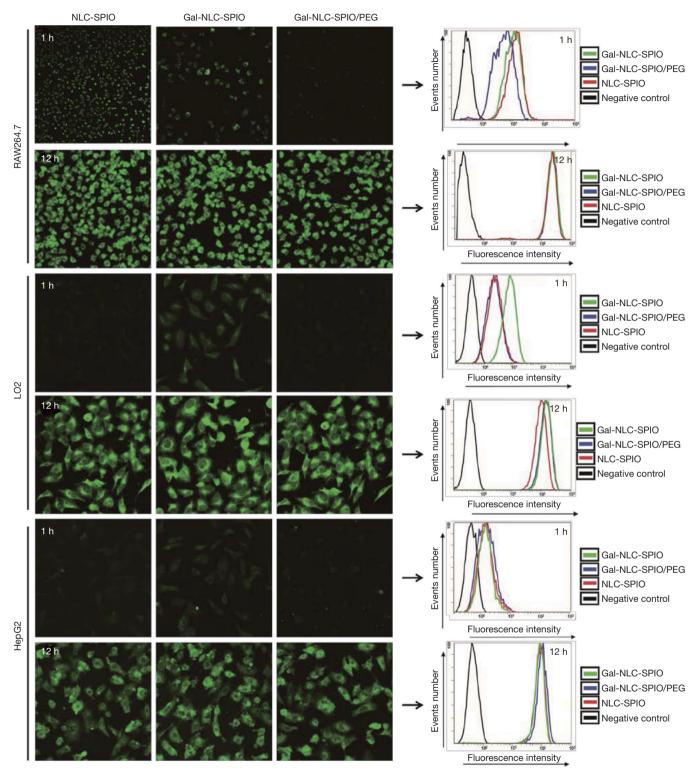
In vitro MR imaging of MNLC

Having magnetic properties is a significant parameter for a MRI contrast agent. In *Figure 5C*, the T2-weighted MRI of Gal-NLC-SPIO shows obvious color change with a variation of Fe_3O_4 concentration. It was found that Gal-NLC-SPIO exhibited good superparamagnetic properties of negative contrast enhancement. The relaxation rate, $R2 = 1/T2$, linearly proportional to the Fe concentration, is also shown in *Figure 5C*. It was indicated in the experiment that Gal-NLC-SPIO exhibited good contrast effect.

T2-weighted images of Gal-NLC-SPIO, NLC-SPIO and Gal-NLC-SPIO/PEG, incubated with HepG2 and LO2 cells for 1 h, along with their signal intensity, are shown in *Figure 5D*. The most apparent decrease in signal density can be seen in the Gal-NLC-SPIO incubated with LO2 cells (*Figure 5E*), and the Gal-NLC-SPIO/LO2 cells showed significant differences in contrast to the other groups ($P<0.01$). This may be attributed to the specific targeting ability of Gal-NLC-SPIO nanoparticles to LO2 cells, leading to the overexpression of cell surface receptors and for the receptor-mediated endocytosis to enhance the uptake into hepatocytes (30).

In vivo MRI of MNLC and pathology studies

Orthotopic implantation hepatoma models were used for

776

Zhu et al. A new MRI contrast agent

Figure 4 *In vitro* cellular uptake of MNLC in different cell lines. Fluorescence images observed by confocal microscopy and fluorescence intensity inside cells measured by flow cytometry of LO2, HepG2 and RAW264.7 cells incubated with FITC-Gal-NLC-SPIO, FITC-NLC-SPIO and FITC-Gal-NLC-SPIO/PEG for 1 h and 12 h, respectively. MNLC, magnetic nanostructured lipid carrier; Gal-NLC, galactose-conjugated nanostructured lipid carrier; SPIO, superparamagnetic iron oxide.
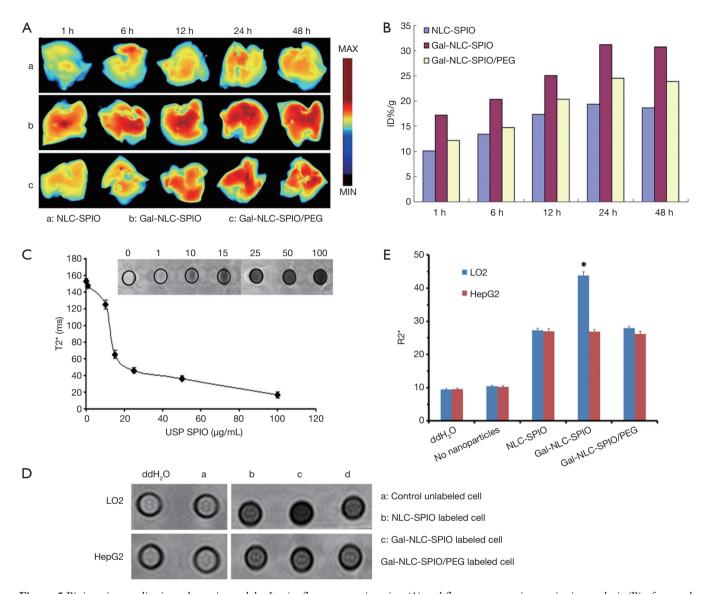
Figure 5 Bioimaging studies in orthotopic models. *In vivo* fluorescence imaging (A) and fluorescent semi-quantitative analysis (B) of normal nude mice liver after intravenous injection of DiR labled NLC-SPIO, Gal-NLC-SPIO and Gal-NLC-SPIO/PEG at different times. MR imaging of magnetic NLCs *in vitro*. (C) T2-weighted images of Gal-NLC-SPIO at different iron concentrations and the chart of T2* values of Gal-NLC-SPIO changing with iron concentrations. (D) LO2 cells or HepG2 cells were incubated with three different kinds of magnetic NLCs for 1 h, and then scanned with MRI. (E) R2* values of LO2 cells or HepG2 cells in different groups were measured (*P<0.01). Gal-NLC, galactose-conjugated nanostructured lipid carrier; SPIO, superparamagnetic iron oxide.

in vivo MRI studies. T2-weighted images of tumor models were obtained before and after intravenous injection of Gal-NLC-SPIO, NLC-SPIO and Gal-NLC-SPIO/PEG, respectively (*Figure 6A*), and the contrast-to-noise ratio (CNR) of T2-weighted MR signal intensity of the tumors are shown in *Figure 6B*. The results produced several significant observations: the liver images of the post-

injection of three MNLCs for 0.5 and 3 h became darkened obviously in contrast with that of pre-injection of MNLC, the CNR of T2-weighted images intensity of livers were obviously decreased (P<0.05), and no significant difference was observed in the CNR of the T2-weighted images intensity of tumors between pre-injection and post-injection of MNLC (P>0.05). Thus, the CNR of the tumor-liver was
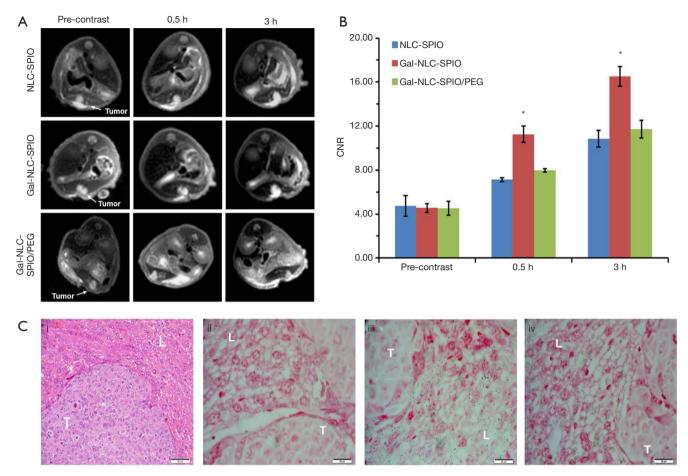
Figure 6 MR imaging and biodistribution studies. (A) T2-weighted single shot fast spin echo images of nude mice bearing HepG2 orthotopic implantation tumor before contrast and at 0.5 and 3 h postinjection of three kinds of MNLC, respectively. The pink arrow stands for tumors. (B) Comparison of CNR of tumor-liver of the three group nude mice at different time points before and after contrast. (C) Microscopic view of HE stained tumor tissue section from nude mice bearing HepG2 tumor (i, magnification: ×400); Prussian blue-stained tumor-liver tissue section of nude mice treated with NLC-SPIO (ii), Gal-NLC-SPIO (iii) and Gal-NLC-SPIO/PEG (iv), respectively (ii, iii and iv, magnification: ×1,000). "L" stands for the normal liver, "T" stands for the tumor. MNLC, magnetic nanostructured lipid carrier; CNR, contrast-to-noise ratio; Gal-NLC, galactose-conjugated nanostructured lipid carrier; SPIO, superparamagnetic iron oxide.

significantly increased after the injection of the Gal-SLN-SPIO compared with those of NLC-SPIO and Gal-NLC-SPIO/PEG (P<0.05), indicating that the Gal-SLN-SPIO shows active targeting ability to normal liver tissues.

The accumulation of iron in tumor tissues and normal liver tissues were further verified. As shown in the first image in *Figure 6C*, the tumor cells were larger and pleomorphic with bigger nucleus and abundant cytoplasm, which indicates that the establishment of orthotopic implantation hepatoma models were successful. More iron could be detected in the liver tissues of the Gal-NLC-SPIO injected group (the third image in *Figure 6C*) than

that of the NLC-SPIO and Gal-NLC-SPIO/PEG injected groups (the second and forth images in *Figure 6C*). These results indicate that Gal-NLC-SPIO has the more effective targeting ability to liver tissues in contrast to NLC-SPIO or Gal-NLC-SPIO/PEG. This can be primarily attested by the fact that Gal-NLC-SPIO successfully inherited the ability to specifically target LO2 liver cells.

Discussion

ASGPR is a specific endocytotic receptor of mammalian hepatocytes, which has a predetermined selectivity for

oligosaccharide or oligosaccharide protein of galactose residues from the end of the molecule in the circulation. Therefore, galactose-modified MNLCs can be applied as a hepatocyte-targeted nano-drug delivery system. Because it has significant clinical value for evaluation of liver disease, it is important to determine if this delivery system is effective and safe. In this study, the novel liver-targeted MRI contrast agents Gal-NLC-SPIO exhibited very low acute toxicity and reasonably good biocompatibility. The results suggest that SPIO loading does not affect the biosafety of the MNLCs. Moreover, the study also found that Gal-NLC-SPIO uptake by LO2 cells was significantly higher and easier than Gal-NLC-SPIO/PEG and free Gal *in vitro* due to the specific interaction between and ASGPR on hepatocytes. Interestingly, Gal-NLC-SPIO uptake by HepG2 cells is relatively rare (*Figures 3-6*), this can be attributed to: (I) the narrow size distribution and biocompatible of Gal-NLC-SPIO (*Figure 2*); (II) and the targeted modification with galactose ligand, which enabled it to specifically internalize into LO2 cells and greatly enhance the hepatocyte targeting by the EPR effect and selective binding of ASGPR (*Figure 3*). However, ASGPR expression of hepatocytes remained at a very low level in disease states, thus resulting in the relatively weak targeting capabilities of Gal-NLC-SPIO in HepG2 cells. Due to the significant difference of Gal-NLC-SPIO in cellular internalization and MRI between LO2 and HepG2 cells, it is possible that Gal-NLC-SPIO shows promise as a novel MRI contrast agent for diagnosis of liver disease.

In this study, Gal-ODA graft was synthesized successfully, and formed MNLC in aqueous solution for the delivery of SPIO. The Gal-NLC-SPIO nanoparticles were effectively consolidated in the liver tissue, due to the targeting peptide Gal-enhanced endocytosis of the nanoparticles. The results of *in vitro* and *in vivo* studies indicated that Gal-NLC-SPIO has a better targeting ability to liver compared with NLC-SPIO and Gal-NLC-SPIO/PEG. Our research shows that, with the mediation of targeting peptide Gal, the Gal-NLC-SPIO has potential for liver-targeting molecular imaging. Therefore, Gal-NLC-SPIO is especially promising as a liver-targeted molecular MRI contrast agent for further clinical utilization.

Acknowledgements

Footnote

Conflicts of Interest: The authors have no conflicts of interest to declare.

References

1. Gong M, Yang H, Zhang S, Yang Y, Zhang D, Li ZH, Zou lg. Targeting T1 and T2 dual modality enhanced magnetic resonance imaging of tumor vascular endothelial cells based on peptides-conjugated manganese ferrite nanomicelles. Int J Nanomedicine 2016;11:4051-63.
2. Terreno E, Castelli DD, Viale A, Aime S. Challenges for molecular magnetic resonance imaging. Chem Rev 2010;110:3019-42.
3. Xie J, Liu G, Eden HS, Ai H, Chen XY. Surface-engineered magnetic nanoparticle platforms for cancer imaging and therapy. Acc Chem Res 2011;44:883-92.
4. Major JL, Meade TJ. Bioresponsive, cell-Penetrating, and multimeric MR contrast agents. Acc Chem Res 2009;42:893-903.
5. Wáng YX, Idee JM. A comprehensive literatures update of clinical researches of superparamagnetic resonance iron oxide nanoparticles for magnetic resonance imaging. Quant Imaging Med Surg 2017;7:88-122.
6. Hasserodt J, Kolanowski JL, Touti F. Magnetogenesis in water induced by a chemical analyte. Angew Chem Int Ed Engl 2014;53:60-73.
7. Lu J, Ma S, Sun J, Xia C, Liu C, Wang Z, Zhao X, Gao F, Gong Q, Song B, Shuai X, Ai H, Gu Z. Manganese ferrite nanoparticle micellar nanocomposites aivs MRI contrast agent for ler imaging. Biomaterials 2009;30:2919-28.
8. Lee SH, Kim BH, Na HB, Hyeon T. Paramagnetic inorganic nanoparticles as T1 MRI contrast agents. Wiley Interdiscip Rev Nanomed Nanobiotechnol 2014;6:196-209.
9. Na HB, Song IC, Hyeon T. Inorganic nanoparticles for MRI contrast agents. Adv Mater 2009;21:2133-148.
10. Wu W, Wu ZH, Yu TY, Jiang CZ, Kim WS. Recent progress on magnetic iron oxide nanoparticles: synthesis, surface functional strategies and biomedical applications. Sci Technol Adv Mater 2015;16:023501.
11. Ghazani AA, Pectasides M, Sharma A, Castro CM, Mino-Kenudson M, Lee H, Shepard JA, Weissleder R. Molecular characterization of scant lung tumor cells using iron-oxide nanoparticles and micro-nuclear magnetic resonance.

Nanomedicine 2014;10:661-8.

12. Li J, He Y, Sun WJ, Luo Y, Cai HD, Pan YQ, Shen MW, Xia JD, Shi XY. Hyaluronic acid-modified hydrothermally synthesized iron oxide nanoparticles for targeted tumor MR imaging. Biomaterials 2014;35:3666-77.

13. De Jong WH, Borm PJ. Drug delivery and nanoparticles: applications and hazards. Int J Nanomedicine 2008;3:133-49.

14. Binnemars-Postma K, Storm G, Prakash J. Nanomedicine Strategies to Target Tumor-Associated Macrophages. Int J Mol Sci 2017;18:E979.

15. Ngambenjawong C, Cieslewicz M, Schellinger JG, Pun SH. Synthesis and evaluation of multivalent M2pep peptides for targeting alternatively activated M2 macrophages. J Control Release 2016;224:103-11.

16. Du YZ, Cai LL, Liu P, You J, Yuan H, Hu FQ. Tumor cells-specific targeting delivery achieved by A54 peptide functionalized polymeric micelles. Biomaterials 2012;33:8858-67.

17. Chaudhary S, Garg T, Murthy RSR, Goyal GAK. Development, optimization and evaluation of long chain nanolipid carrier for hepatic delivery of silymarin through lymphatic transport pathway. Int J Pharm 2015;485:108-21.

18. Situ JQ, Wang XJ, Zhu XL, Xu XL, Kang XQ, Hu JB, Lu CY, Ying XY, Yu RS, You J, Du YZ. Multifunctional SPIO/DOX-loaded A54 Homing Peptide Functionalized Dextran-g-PLGA Micelles for Tumor Therapy and MR Imaging. Sci Rep 2016;6:35910.

19. Shidhaye SS, Vaidya R, Sutar S, Patwardhan A, Kadam VJ. Solid lipid nanoparticles and nanostructured lipid carriers-innovative generations of solid lipid carriers. Curr Drug Deliv 2008;5:324-31.

20. Yingchoncharoen P, Kalinowski DS, Richardson DR. Lipid-Based Drug Delivery Systems in Cancer Therapy: What Is Available and What Is Yet to Come. Pharmacol Rev 2016;68:701-87.

21. Beloqui A, Solinis MA, Rodriguez-Gascon A, Almeida

AJ, Preat V. Nanostructured lipid carriers: Promising drug delivery systems for future clinics. Nanomedicine 2016;12:143-61.

22. Khan S, Baboota S, Ali J, Khan S, Narang RS, Narang JK. Nanostructured lipid carriers: an emerging platform for improving oral bioavailability of lipophilic drugs. Int J Pharm Investig 2015;5:182-91.

23. Iqbal MA, Md S, Sahni JK, Baboota S, Dang S, Ali J. Nanostructured lipid carriers system: recent advances in drug delivery. J Drug Target 2012;20:813-30.

24. Lu W, He LC, Wang CH, Li YH, Zhang SQ. The use of solid lipid nanoparticles to target a lipophilic molecule to the liver after intravenous administration to mice. Int J Biol Macromol 2008;43:320-4.

25. Maeda H, Nakamura H, Fang J. The EPR effect for macromolecular drug delivery to solid tumors: Improvement of tumor uptake, lowering of systemic toxicity, and distinct tumor imaging in vivo. Adv Drug Deliv Rev 2013;65:71-9.

26. Lee CM, Jeong HJ, Kim SL, Kim EM, Kim DW, Lim ST, Jang KY, Jeong YY, Nah JW, Sohn MH. SPION-loaded chitosan-linoleic acid nanoparticles to target hepatocytes. Int J Pharm 2009;371:163-9.

27. Wang W, Zhao XL, Hu HY, Chen DW, Gu JC, Deng YH, Sun J. Galactosylated solid lipid nanoparticles with cucurbitacin B improves the liver targetability. Drug delivery 2010;17:114-22.

28. Craparo EF, Sardo C, Serio R, Zizzo MG, Bondi ML, Giammona GG. Galactosylated polymeric carriers for liver targeting of sorafenib. Int J Pharm 2014;466:172-80.

29. Yuan H, Miao J, Du YZ, You J, Hu FQ, Zeng S. Cellular uptake of solid lipid nanoparticles and cytotoxicity of encapsulated paclitaxel in A549 cancer cells. Int J Pharm 2008;348:137-45.

30. Lian J, Zhang S, Wang J, Fang K, Zhang Y, Hao Y. Novel galactosylated SLN for hepatocyte-selective targeting of floxuridinyl diacetate. J Drug Target 2008;16:250-6.
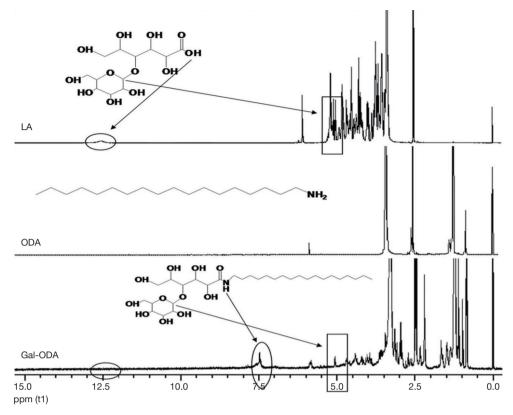
Figure S1 ^{1}H NMR spectra of LA, ODA and Gal-ODA.

Table S1 Particle diameter and zeta potential of NLC-SPIO, Gal-NLC-SPIO and Gal-NLC-SPIO/PEG. Data represent the mean ± standard deviation (n=3)

Sample	Diameter (nm)	PI (–)	Zeta potential (mV)
NLC-SPIO	52.60±5.74	0.24±0.09	−28.45±1.20
Gal-NLC-SPIO	53.47±3.39	0.24±0.08	−30.68±1.10
Gal-NLC-SPIO/PEG	55.87±5.81	0.19±0.05	−33.72±1.28

Gal-NLC, galactose-conjugated nanostructured lipid carrier; SPIO, superparamagnetic iron oxide.
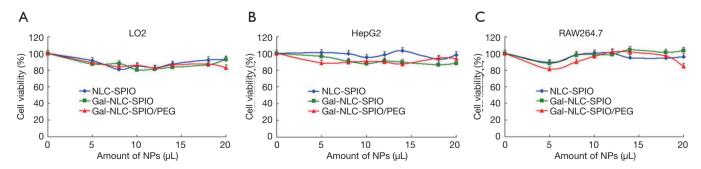

Figure S2 *In vitro* cytotoxicity of NLC-SPIO, Gal-NLC-SPIO and Gal-NLC-SPIO/PEG against LO2 (A), HepG2 (B) and RAW264.7 (C) cells, respectively. Data represent the mean ± standard deviation (n=3). Gal-NLC, galactose-conjugated nanostructured lipid carrier; SPIO, superparamagnetic iron oxide.